Exploring the limitations of osmotically assisted reverse osmosis: Membrane fouling and the limiting flux

Christian D. Peters [a,b,1], Dan Li [b,c,1], Zijing Mo [b,c,d], Nicholas P. Hankins [a,*], Qianhong She [b,c,*]

[a] Department of Engineering Science, The University of Oxford, Parks Road, OX3 1PJ, Oxford, UK

[b] Singapore Membrane Technology Centre, Nanyang Environment & Water Research Institute, Nanyang Technological University, Singapore 637141, Singapore

[c] School of Civil and Environmental Engineering, Nanyang Technological University, 50 Nanyang Avenue, Singapore 639798, Singapore

[d] Interdisciplinary Graduate Programme, Nanyang Technological University, 50 Nanyang Avenue, Singapore 639798, Singapore

[1] These authors contributed equally to this work

* Corresponding authors

Email address: nick.hankins@eng.ox.ac.uk (N.P. Hankins); qhshe@ntu.edu.sg (Q. She)

Abstract

Osmotically assisted reverse osmosis (OARO) has shown a great potential for low-cost and energy-efficient brine management. However, its performance can be significantly limited by membrane fouling. Here, we performed for the first time a comprehensive study on OARO membrane fouling, explored the associated fouling mechanisms, and evaluated fouling reversibility via simple physical cleaning strategies. Firstly, internal membrane fouling at the draw (permeate) side was shown to be insignificant. Flux behaviour in short-term operation was correlated to both the evolution of fouling and the change of internal concentration polarization. In long-term operation, membrane fouling constrained the OARO water flux to a singular, common upper limit, in terms of limiting flux, which was demonstrated to be independent of operating pressures and membrane properties. Generally, once the limiting flux was exceeded, the OARO process performance could not be improved by higher pressure operation or by utilising more permeable and selective membranes. Instead, different cyclic cleaning strategies were shown to be more promising alternatives for improving performance. While both surface flushing and osmotic backwashing (OB) were found to be highly effective when using pure water, a full flux recovery could not be achieved when a non-pure solution was used during OB due to severe internal clogging during OB. All in all, the presented findings provided significant implications for OARO operation and fouling control.

Keywords: osmotically assisted reverse osmosis, membrane fouling, limiting flux, internal concentration polarization (ICP), ICP self-compensation effect, fouling reversibility

Synopsis: The performance of osmotically assisted reverse osmosis for brine disposal is demonstrated to be constrained by coupled effects of fouling and internal concentration polarization.

Graphical Abstract

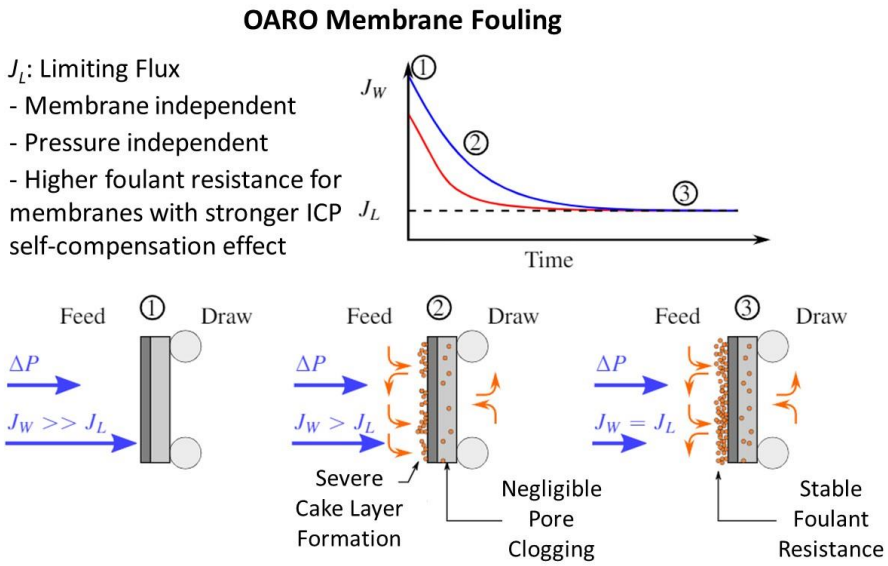

1. Introduction

The potential of osmotically assisted reverse osmosis (OARO) to provide low-cost and energy efficient brine volume minimisation has been proven by several numerical studies [1–7]. In comparison to other well-established high-recovery membrane processes, such as high-pressure reverse osmosis (HPRO) and forward osmosis (FO), OARO gains its competitive advantage by having a saline sweep on the permeate side to reduce the transmembrane osmotic pressure difference, enabling high recovery desalination while operating at a hydraulic pressure that does not exceed the membrane burst pressure. Numerical estimates of the achievable OARO brine concentration are exemplary and can reach up to 205 g/kg [5] and 245 g/kg [6]. In practice, however, the performance of OARO processes is expected to be inevitably affected by membrane fouling, which has not been systematically examined to date.

OARO is susceptible to both severe membrane deformation [8] and fouling, as OARO membranes (1) are exposed to high hydraulic pressures, (2) ideally have a thin substrate to minimise internal concentration polarisation (ICP), and (3) are used to treat highly concentrated solutions with impurities. In comparison to other membrane desalination processes, OARO can utilise the same feed and draw solution which can contain a range of organic and inorganic fouling species and may vary from wastewater [9], seawater to concentrated brine [1–5]. Hence, fouling on both sides of the OARO membrane is highly likely. Of special concern is internal membrane fouling on the draw side, where pore clogging can occur if foulants enter the membrane's porous substrate [10]. In this case, fouling enhanced ICP would substantially lower the OARO water flux. Depending on the chosen draw solution, internal membrane fouling in FO in AL-FS mode was found to be either significant [11] or not [12] and hence, deserves experimental investigation in OARO. Although the permeate water flow also opposes the accumulation of foulants within the membrane substrate, high pressure operation is expected to significantly change the hydrodynamic conditions within the OARO draw channel.

Compaction of the membrane and its spacer support narrow the flow channels, which can lead to enhanced foulant deposition and plugging of the spacer [13,14] and potentially of the membrane.

Significant foulant accumulation on a pristine membrane and the associated flux reduction are predicted to occur, once the water flux exceeds the so-called critical flux [15,16]. The critical flux is not fixed and depends on the foulant-membrane interactions, which are related to the feedwater properties, membrane characteristics and operational conditions. However, under extreme fouling conditions, as often faced in OARO processes, the entire membrane surface can be potentially covered by foulants. Once this happens, the fouling development is independent of the pristine membrane properties, as shown by Tang et al. [17]. Similar results were observed in other studies [18,19] and it was shown that the water flux after long-term fouling tended to achieve an identical pseudo-stable value, termed the limiting flux. While the limiting flux was shown to be independent of the membrane properties in RO [17,20] and FO [21] (AL-FS mode), this may not, however, be the case for OARO if internal membrane fouling is a concern. For example, in pressure retarded osmosis (PRO) the limiting flux was shown to be dependent on the membrane's structural parameter *S* when scaling within the membrane substrate was substantial [22,23]. It is necessary to examine how the operating pressure and membrane properties influence the limiting flux in OARO and further to gain an understanding of the technical implications for OARO operation.

As OARO exhibits certain similarities to FO, dilutive ICP at the draw side will significantly reduce the effective driving force and thus result in a lower-than-expected flux [8]. On the other hand, several studies on FO fouling reported that flux remained relatively stable during membrane fouling in AL-FS mode due to the ICP self-compensation effect [24–26]. Tang et. al [27] related this observation to the fact that any minute reduction in the membrane's water flux due to fouling will immediately be counterbalanced by a reduction in ICP, and hence, will result in a milder reduction of the membrane's water flux. While the ICP self-compensation

effect is presumably applicable as well in OARO, it is important to investigate how it affects the OARO flux behaviour during fouling.

As laid out in this paper, several complex and interdependent mechanisms of membrane fouling may occur during OARO operation. The objective of this study is to explore these mechanisms and to gain a better understanding of the technical limitations of OARO. This study covers a detailed investigation into the effects on the OARO process performance of the feed and draw compositions, the membrane properties and the hydraulic pressure. Additionally, possible membrane cleaning methods, such as osmotic backwashing and surface flushing, are evaluated for their efficacy in alleviating fouling and restoring the membrane's initial water flux.

2. Materials and Methods

2.1. Membranes and spacer backing

Two commercially available membranes, namely an aquaporin (AQP) based TFC membrane from Aquaporin A/S (Copenhagen, Denmark) and a FilmTec flat-sheet brackish water RO membrane (BW30LE), were used in this study to investigate OARO fouling. Both membranes were considered to be suitable OARO membranes and were already fully characterised at operating pressures of up to 60 bar [8]. The membranes were stored at 4°C and extensively rinsed and soaked in Milli-Q water for over 24 hours before use.

A 3D printed spacer and a tricot-type RO permeate carrier, which was obtained from a commercial RO spiral wound module [28], were also used in this study. To reduce the spacer openings, the RO permeate carrier was placed on top of the 3D printed spacer to further improve the membrane's support structure. This spacer backing used in the draw channel could fully support the membranes at operating pressures of up to 60 bar [8]. More information on the 3D printed spacer is given in Peters et al. [8]. No feed spacer was used in the membrane fouling experiments to accelerate fouling.

2.2. Chemicals and solutions

OARO membrane fouling was investigated using five different combinations of feed and draw solutions. Unless otherwise stated, all solutions were prepared with ACS grade chemicals/reagents and prepared using ultra-pure water. All draw and feed solutions were calculated to have a comparable osmotic pressure of approximately 35 bar using OLI Studio 10.0 software (OLI Systems Inc., Morris Plains, NJ). The compositions of the synthetic solutions are stated in Table 1. The inorganic precipitates that were added in F2, F3 and F4 were purchased from Sigma Aldrich and were calcium carbonate and calcium sulfate dihydrate with both having a mean size of approximately 325 mesh.

As dosing the feed and draw solutions was deemed unnecessary and impractical, a reference case (RC), with pure NaCl feed and draw solutions, was used to record the water flux reduction that was solely caused by the changes of the concentrations of feed and draw solutions during OARO operation (i.e., due to feed concentration and draw dilution). Firstly, the effects of membrane scaling on the OARO process performance were investigated using test case F1. Inorganic fouling can be a serious concern for seawater and brackish water desalination. Typically, the most common scaling constituents in seawater are calcite ($CaCO_3$) and gypsum ($CaSO_4 \cdot 2H_2O$) [29]. Therefore, calcite [30–32] and gypsum [33–35] scaling have been widely studied for a variety of membrane processes. As OARO is generally utilised to concentrate RO brines [4], the concentrations of gypsum and calcite precursor ions were chosen to be representative of those present in seawater RO brines (at 50% recovery) [14,36]**.** The saturation index (SI) of gypsum and calcite in F1 were calculated using OLI Studio 10.0 software and are -0.14 and 0.73, respectively. For supersaturated solutions (SI>0), scale formation is a likely phenomenon [37,38] which may inevitably cause a flux reduction in OARO. For test case F2, gypsum and calcite precipitates were directly added to the feed and draw solutions to investigate whether the presence of already formed precipitates in the bulk solutions would enhance membrane fouling.

148 Test cases F3 to F5 investigate organic fouling in the presence of calcium ions. Sodium alginate
149 is chosen in this study as a model foulant due to its ubiquity in surface waters and its known
150 strong interaction with calcium ions [14]. In F3, sodium alginate is only added to the draw side
151 to determine whether organic fouling on the OARO membrane's draw side is significant or
152 not. On the other hand, in test cases F4 and F5 sodium alginate is also added to the feed solution.
153 The inorganic precipitates (calcite and gypsum crystals) are also added to both feed and draw
154 in test case F4 to simulate the OARO process under the most extreme fouling conditions.

155

Table 1: Composition of the synthetic feed and draw solutions used for the OARO fouling experiments.

Test Case [a]	RC	F1	F2	F3	F4	F5
Feed composition (mmol/L)						
NaCl	750	600	600	600	600	600
$CaCO_3$(s)	0	0	0.25	0	0.25	0
$CaSO_4$ (s)	0	0	11	0	11	0
$CaCl_2$ [b]	0	21.62	21.62	21.62	21.62	21.62
Na_2SO_4 [b]	0	57.75	57.75	57.75	57.75	57.75
$NaHCO_3$ [b]	0	4.76	4.76	4.76	4.76	4.76
Alginate [c]	0	0	0	0	0.46	0.46
Draw composition (mmol/L)						
NaCl	750	600	600	600	600	600
$CaCO_3$ (s)	0	0	0.25	0.25	0.25	0
$CaSO_4$ (s)	0	0	11	11	11	0
$CaCl_2$ [b]	0	21.62	21.62	21.62	21.62	21.62
Na_2SO_4 [b]	0	57.75	57.75	57.75	57.75	57.75
$NaHCO_3$ [b]	0	4.76	4.76	4.76	4.76	4.76
Alginate [c]	0	0	0	0.46	0.46	0.46

[a] RC: Reference case, only NaCl present in the solutions; F1: Scaling precursors dissolved in both feed solution (FS) and draw solution (DS), neither crystals nor alginate present in bulk solutions; F2: Crystals present in bulk solutions and scaling precursors dissolved in both FS and DS; F3: scaling precursors dissolved in both FS and DS, alginate dissolved in DS only and crystals present in DS only; F4: Crystals present in bulk solutions and scaling precursors and alginate dissolved in both FS and DS; F5: Scaling precursors and alginate dissolved in both FS and DS and no crystal present in bulk solutions.

[b] Concentrations calculated based on a 50% recovery of a seawater RO plant [14,36].

[c] Alginate concentration is 100 mg/L (MW: 216 g/mol).

2.3. OARO fouling experiments

All fouling experiments were carried out in a Sterlitech membrane test cell that can withstand operating pressures of up to 69 bar. The digital pressure gauges were only calibrated for operating pressures of up to 60 bar, which was therefore set as maximum pressure for all tests performed. The test-rig utilised in this study is described in detail in She et al. [14]. As previously mentioned, no dosing pumps were utilised during the fouling experiments. The temperature of the pressurised feed solution was kept constant at 25±1 °C using a cooling coil.

Prior to the addition of alginate in test cases F3-F5, the membrane was firstly compacted using the alginate-free feed and draw solutions at the required operating pressure for 30 min to ensure that any sudden flux reduction was solely caused by membrane fouling and not by membrane deformation. The duration of each fouling experiment was approximately 4 hours with the water flux J_W, operating pressure ΔP and the feed and draw conductivities recorded in 10-second intervals. For all experiments, the cross-flow velocity (CFV) was set as 10 cm/s in both feed and draw channels [8].

To ensure repeatability and an accurate analysis of the presented results, each AQP fouling scenario in Figure 2 was repeated twice, except for F2 due to limited AQP membrane coupons in the same batch available in stock. Two BW30LE experiments were also carried out for each different operating pressure investigated in Figure 4 to ensure repeatability of the results.

2.4. OARO cleaning experiments

As shown in Figure 1, three different cleaning strategies were investigated in this study. Flushing the fouled membrane using deionised (DI) water constituted the first. The other two cleaning strategies for OARO focussed on osmotic backwashing (OB) using different feed and draw solutions. The ideal OB strategy would use a deionised draw solution whereas the real OB utilised a synthetic seawater solution as draw. The three cleaning strategies modelled the

use of either product water or less expensive feedwater (i.e., seawater) as possible cleaning solutions to determine their efficacy. The organic fouling experiments (F5) were repeated three times, each lasting approximately 80 minutes to give a total fouling duration of 4 hours. In between the fouling cycles, cleaning cycles were carried out and lasted for approximately 10 minutes.

Flushing the fouled membrane using deionised (DI) water constitutes the first strategy. A cross-flow velocity (CFV) of 20 cm/s was chosen in our flushing experiments, which is similar to the CFV used by Mi and Elimelech [39] and Vu et al. [40]. The flow direction was not altered during membrane cleaning. The other two cleaning strategies for OARO focus on osmotic backwashing using different feed and draw solutions. In comparison to flushing, a reverse water flux is induced during OB that can theoretically enhance the dissociation and dislodging of the fouling layer from the membrane's active layer [41]. To enhance the reverse water flux, the operating pressure is reduced in both OB cleaning scenarios to approximately zero. In practice, however, osmotic backwashing can be used on-line, without stopping the high-pressure pumps [42,43]. In addition, OB is a rapid cleaning method that is also membrane and environmentally friendly, as no additional cleaning chemicals are used.

In the ideal OB scenario, deionised water is used as draw solution, whereas a pure 2.4 M NaCl solution is used as feed solution. This case is deemed ideal, as no foulants are present in either draw or feed solution, and the transmembrane hydraulic pressure is at a minimum, meaning that the maximum reverse water flux can be achieved. The 2.4 M NaCl solution reflects the salinity achievable by OARO membrane processes [4,5]. Hence, the OARO brine could be ideally used for the OB procedure without incurring any additional cost. However, using deionised water during the OB or flushing process is costly, as the OARO/RO product water must be utilised for this. To circumvent using DI water for the OB process, a more realistic OB scenario is also investigated in this study. Instead of using DI water, the original draw solution from test

case F5 is utilised in the real OB scenario to simulate on-line OB. Furthermore, the feed solution is chosen to resemble OARO brine with organics (100 mg/L alginate) and ion concentrations 3.2 times higher than the concentrations specified for the F5 feed solution.

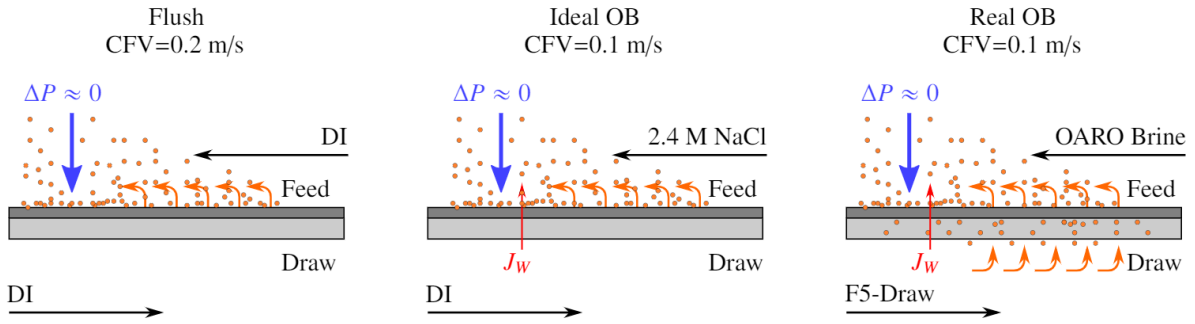

Figure 1: The three different cleaning scenarios investigated.

2.5. Effective driving force and foulant resistance

The effective driving force (DF_{Eff}) of OARO can be described using the osmotic resistance filtration model as follows [8,10]:

$$DF_{Eff} = (\Delta P - \Delta\pi) - f_{CCP}\left(\pi_F - \frac{J_S}{J_W}\beta R_G T\right) - f_{DCP}\left(\pi_D - \frac{J_S}{J_W}\beta R_G T\right) \quad (1)$$

where ΔP, $\Delta\pi$, π_F and π_D are the transmembrane hydraulic pressure difference, the apparent osmotic pressure difference between draw and feed solutions, the feed osmotic pressure and draw osmotic pressure, respectively. J_W, J_S, β, R_G and T are the water flux, solute flux, van't Hoff factor, the universal gas constant and the solution temperature, respectively f_{CCP} and f_{DCP} are the concentrative and dilutive concentration polarisation factors, respectively, and are given below:

$$\begin{cases} f_{CCP} = e^{\frac{J_W}{k_F}} - 1 \\ f_{DCP} = 1 - e^{-\frac{J_W S}{D}} \end{cases} \quad (2)$$

where k_F, S and D are the mass transfer coefficient near the membrane active layer surface at the feed side, the membrane's structural parameter S and the solute diffusivity.

The foulant resistance R_F can be calculated using [26]:

$$J_W = \frac{DF_{Eff}}{\mu(R_M + R_F)} \quad (3)$$

where μ is the fluid viscosity and $1/\mu R_M$ is the same as the water permeability A of the pristine membrane.

3. Results and discussion

3.1. Effect of feed and draw solution composition on OARO fouling

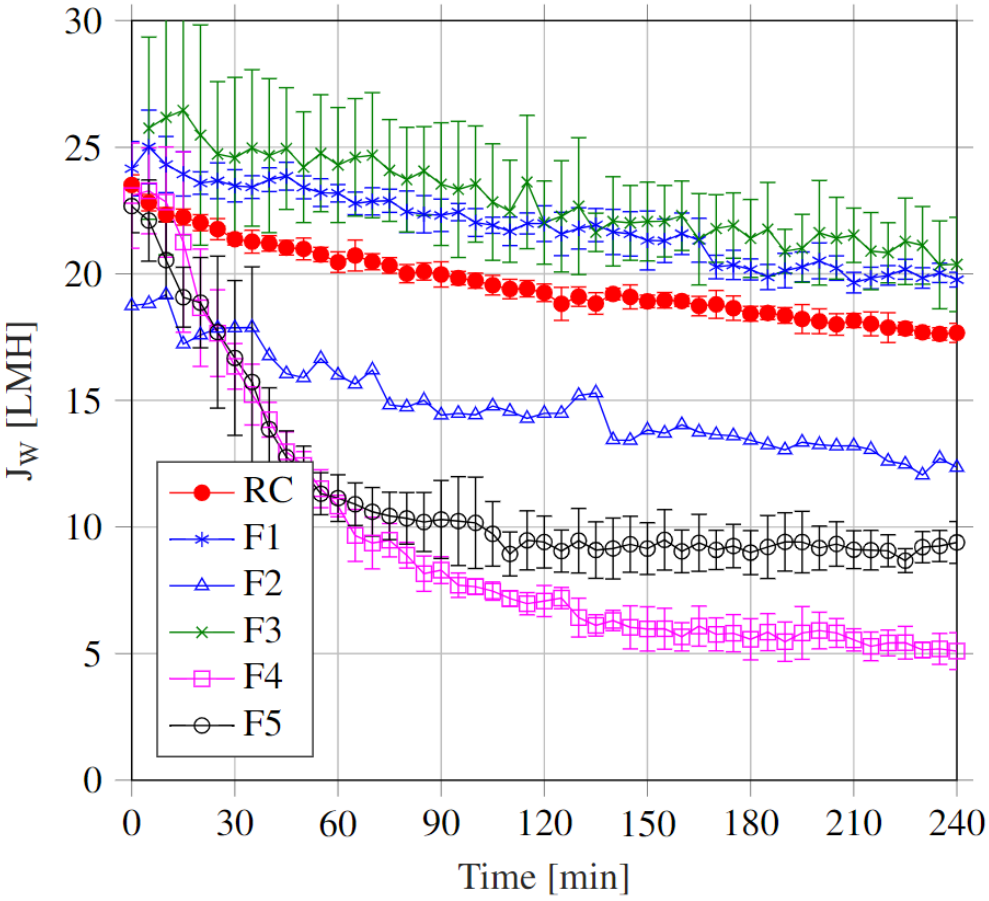

Figure 2: Effect of feed and draw solution composition on OARO permeate flux evolution. All fouling experiments were carried out using the AQP membrane at 50 bar with cross-flow velocity of 10 cm/s. RC: Reference case, and solution compositions for F1-F5 are listed in Table 1.

Figure 2 shows the water flux results obtained for the reference case (RC) and the five fouling scenarios with different FS and DS compositions. All experiments were performed with the AQP membrane at a constant operating pressure of 50 bar. This resulted in an initial flux of

approximately 22-24 LMH for all tests. The water flux of the RC reduced from an initial water flux J_0 of 23 LMH down to 18 LMH after a 4-hour OARO operation. This flux reduction is caused by the increasing transmembrane osmotic pressure difference, as the feed solution was concentrated, and the draw solution was diluted.

The reference case is simulated for both the AQP and BW30LE membrane and compared to the experimental findings in section S1 of the supporting information. The simulation results show that the flux reduction is caused by the increasing transmembrane osmotic pressure difference as the feed and draw concentrations were changed by more than 5% over the 4-hour experimental duration. In addition, the simulation of the AQP reference case shows that the OARO sweep solution contributes towards the overall water flux. This shows that at the given feed/draw concentrations and operating fluxes, the AQP membrane is truly operated in OARO mode.

Surface crystallization plays an insignificant role in OARO flux decline. It was observed that the flux for test scenario F1 is similar to that of RC. The inclusion of scale precursor ions in both the feed and draw solutions (test case F1) did not lead to a more severe flux reduction within the 4-hour operational window. Hence, it can be concluded that membrane scaling was not significant under the given operational conditions. Solute precipitation is mainly expected on the membrane's feed side, as the feed solution is continuously concentrated while the draw is diluted. In addition, concentrative external concentration polarisation (ECP) causes higher solute concentrations near the membrane surface and hence, may lead to surface crystallization if the saturation limit is exceeded [44]. In scenario F1, the main scaling precipitates are gypsum (calcium sulphate), which has a relatively high solubility. It is expected that the small amount of gypsum precipitates formed on the membrane surface would be removed at the high crossflow velocity on the feed side. Furthermore, no feed spacer was employed in this study to

prevent any stagnant regions between the feed spacer filaments and the membrane surface, where potential precipitates would form [45].

Under the given feed conditions, the feed concentration at the membrane surface is increased by approximately 13% at 20 LMH due to ECP, which leads to an increase of the calcite and gypsum saturation index above 1. In longer operational periods scaling of the membrane surface is therefore possible.

The current study, however, found that within the given testing time, surface crystallisation is of no significance or may not even occur, which suggests long induction times for the given feed and draw scalants. This issue deserves further investigation in long term operation in future studies.

Bulk crystallization plays a significant role in OARO flux decline. Besides the scale precursor ions, inorganic precipitates were added to the feed and draw solutions in test case F2, which simulates a scenario for which bulk crystallization has already occurred. While the water flux of F1 did not deviate from that of the reference case, the water flux of F2 was substantially lower than that of the reference case after 4 hours. The F2 water flux dropped to 13 LMH. The difference in the J_W trends between F1 and F2 suggests that the additional flux reduction in F2 must be caused by the deposition and agglomeration of the inorganic precipitates on the membrane surface. In general, there are two distinct precipitation pathways in membrane modules, namely surface crystallisation, and bulk crystallisation. Both pathways of crystallisation can occur simultaneously and initiate/aggravate each other [46]. For example, homogeneous crystal formation in the bulk can lead to scale deposition and cake layer formation on the membrane due to their continuous transport towards the membrane surface, which is the dominant scaling mechanism for F2 scenario. Moreover, this cake layer may offer a secondary nucleation site for further scale formation under supersaturated conditions, which further increases the resistance to water transport through the membrane.

Fouling/scaling is insignificant on the draw (permeate) side in OARO. As shown in Figure 2, test case F3 also shows no deviation from the reference case. The objective of test case F3 was to investigate whether organic fouling, scaling and/or inorganic precipitates on the membrane's draw side cause any significant flux decline. As no deviation from the reference case was observed, it can be concluded that fouling on the membrane's draw side is negligible and causes no significant loss in OARO performance. A similar finding was made by Boo et. al [12], who found that internal fouling on the draw side is negligible for forward osmosis processes operated in the AL-FS mode. This is due to the fact that the permeate water flow opposes the accumulation of foulants within the membrane substrate in the AL-FS mode. This is an important finding for OARO operation, as it suggests that membrane fouling is only likely to be a concern on the membrane's feed side. This suggests that untreated solutions can potentially be used directly as OARO draw solution without any concern for membrane fouling. It should be noted that although no OARO internal fouling was observed in AL-FS mode, even when using a draw solution highly concentrated with organic and inorganic foulants, this might not be the case when using other draw solutions (e.g., surfactants [11]) or when operating at lower water fluxes. Zohrabian et al. [11] found that when the foulant's adsorptive and diffusive forces exceeded the counteracting convective forces (i.e., the permeate water flux), internal membrane fouling in FO in AL-FS mode was possible and hence, internal membrane fouling may also be possible in OARO. In addition, while no flux reduction was observed during F3, some organic matter was still observed to be trapped within the tight and compacted draw spacer. Pictures of the plugged draw spacers are shown in the supporting information (refer to S2 in SI). She et al. [14,22] made a similar finding for PRO and found that the compacted feed spacer was plugged by organic material during operation. This means that any precipitates should still be filtered from the draw solution to prevent any pressure loss caused by the plugging of the compacted OARO draw spacer.

Combined organic fouling and inorganic scaling synergistically enhance OARO flux decline. The most severe flux decline was observed for test cases F4 and F5 in which alginate was added in the feed solution and combined organic fouling and inorganic scaling occurred. While the flux decline was similar for both scenarios in the first 2 hours, the final "steady-state" water flux differed. After 4 hours of operation, F4 and F5 reached a water flux of 6 LMH and 9 LMH, respectively. In comparison to test case F3 where only inorganic scaling occurred, the combined organic fouling and inorganic scaling for F4 and F5 led to a more significant flux decline. In F4, inorganic precipitates were also present in both the bulk feed solution and the draw solution. As suggested in other studies, the calcium alginate (Ca-Alg) agglomerates in combination with the inorganic precipitates can form a denser and thicker fouling layer in F4 than the Ca-Alg agglomerates alone in F5 [47,48]. This would explain why the final water flux is lower for F4 than F5. Both test cases suggested that the formation of Ca-Alg agglomerates and their interaction and deposition on the membrane surface cause a severe flux decline. As for any membrane process, organic fouling remains a major challenge and has been widely investigated [10,14,47,49]. The severity of organic fouling in OARO is dependent on a multitude of factors and is mainly related to the feed side properties.

3.2. Pressure-independent limiting flux in OARO

The effects of the operating pressure (i.e., the initial water flux) on the OARO fouling propensity are shown in Figure 3. All presented results were obtained using the AQP membrane and the solution compositions specified for test case F5 (Table 1).

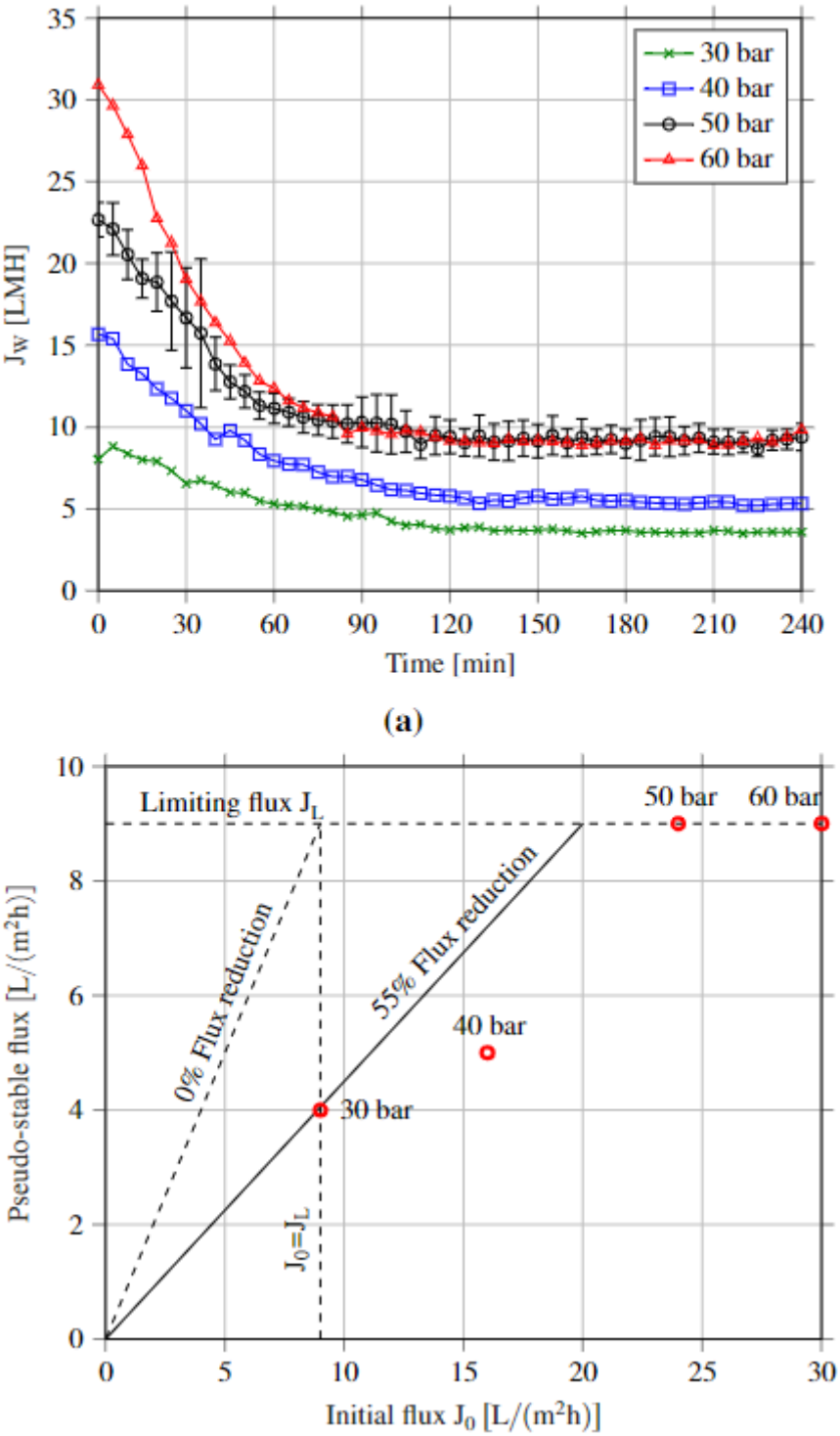

Figure 3: (a) Effect of the applied hydraulic pressure on OARO permeate flux evolution. All fouling experiments were carried out using the AQP membrane using the solutions specified for test case F5 in Table 1. (b) Relationship between the initial and final, pseudo-stable water flux.

As shown in Figure 3 (a), the initial water flux J_0 increased from 10 LMH to 30 LMH when the operating pressure was increased from 30 bar to 60 bar. A higher initial water flux is

associated with a higher fouling rate [15] and hence, a steeper flux reduction was observed at higher operating pressures. A limiting flux can be observed at approximately 9 LMH for the OARO process, above which the membrane flux cannot be sustained. This limiting flux is reached in both of the 50 bar and 60 bar fouling experiments. For a more detailed introduction and derivation of the limiting flux, please refer to S3 in the supporting information.

While the initial water flux at 40 bar (15 LMH) supersedes the limiting flux, the final water flux (5 LMH) is below the limiting flux. This is contrary to the findings of Tang and Leckie [50] who observed a well-defined limiting flux behaviour where (1) almost no flux decline was recorded when the initial flux was less than the limiting flux and (2) the final flux was equivalent to the limiting flux if the initial flux exceeded the limiting flux. In this case, an intermediate state is reached at 40 bar in which the obtained pseudo-stable water flux $J_W^{40\ bar}$ ranges between the critical flux (J_C) and limiting flux (J_L), i.e., $J_C < J_W^{40\ bar} < J_L$. While the critical flux was not directly determined in this study, Bacchin [16] showed that the critical flux is lower than the limiting flux for colloidal systems and hence, the barrier force (repulsive force) between the foulant in the solution and the clean AQP membrane ($F_{\mathrm{Barrier}}^{f-m}$) is expected to be lower than that between the foulant and the formed foulant layer on the membrane ($F_{\mathrm{Barrier}}^{f-f}$). This intermediary state is also observed for the 30 bar fouling experiment. The initial water flux at 30 bar (9 LMH) is equivalent to the observed limiting flux, but the final pseudo-stable water flux (4 LMH) is lower than the limiting flux. For these two scenarios, the barrier forces at the pseudo-stable flux for 30 bar and 40 bar (i.e., $F_{Barrier}^{30\ bar}$ and $F_{Barrier}^{40\ bar}$, respectively) are expected to be:

$$F_{Barrier}^{f-m} < F_{Barrier}^{40\ bar} < F_{Barrier,L}^{f-f} \qquad (4)$$

and:

$$F_{Barrier}^{f-m} < F_{Barrier}^{30\ bar} < F_{Barrier,L}^{f-f} \quad (5)$$

where $F_{Barrier,L}^{f-f}$ is the barrier force offered by the fouled membrane when the limiting flux is reached.

Another phenomenon which could contribute here to the greater flux decline and augment the degree of foulant deposition at higher operating pressures is the diffusiophoresis (DP) effect [26,51]. This effect is expected to be stronger at higher initial water fluxes due to the increase in external concentration polarisation, which may lead to a greater diffusiophoretic gradient within the cake layer. This could lead to greater cake compaction at higher operating pressures and hence, to a greater flux reduction.

The relationship between the initial water flux J_0 and the final pseudo-stable water flux is shown in Figure 3 (b). The intermediary state at 30 bar ($J_C < J_W^{30\ bar} < J_L$) and 40 bar ($J_C < J_W^{40\ bar} < J_L$) is clearly visible from this figure, as in both scenarios the final pseudo stable water flux is below J_L although $J_0 \geq J_L$. It is noted that a similar relationship between the initial water flux and the final pseudo-stable flux was observed by She et al. [52] in the study of ultrafiltration (UF) membrane fouling. She et al. [52] reasoned that this non-ideal, intermediary state occurs due to the non-homogeneity of UF membranes such that localised microscale fluxes can exceed or fall below the apparent macroscale average flux. In regions where local fluxes are higher than the limiting flux, those local fluxes will decline and eventually stabilized at the limiting flux level. Noting that in other regions local fluxes are lower than limiting flux the apparent macroscale average flux in all regions will decline to below the limiting flux.

The non-homogeneity of AQP membranes due to localized variations in the surface roughness and active layer thickness has already been demonstrated by a variety of other studies [53–55]. Thus, it can be hypothesised that membrane fouling is more severe in regions with high local water fluxes, whereas fouling is less severe in regions with lower local water fluxes, causing

the formation of a fouling layer so that $F_{Barrier}^{f-m} < \mathrm{F_{Barrier}} < F_{Barrier,L}^{f-f}$. This explains the greater than expected flux reductions at 30 bar and 40 bar, as the actual barrier force is less than that induced by a fully, homogeneously fouled membrane. On the other hand, it is expected that the AQP membrane is completely covered by a homogeneous foulant layer at operating pressures exceeding 50 bar with a relatively high initial water flux, as the final pseudo stable water fluxes at 50 bar and 60 bar are equivalent to the limiting flux. A foulant resistance analysis was conducted in the supporting information S5 using the results presented in Figure 3. The results indicate that the effective driving force increased with increasing the applied pressures from 30 bar to 60 bar, but foulant resistance at 30 bar exceeded that at 50 and 60 bar due to an increased ICP self-compensation effect at lower water fluxes. This finding on R_F is interesting and will be investigated more systematically in future OARO studies.

This means that for long-term OARO operation, without continuous membrane cleaning, it is not advised to operate the AQP membrane at pressures exceeding 50 bar, as the same limiting flux will be reached under the given feed conditions. In essence, an energy saving of 16.7% can be achieved by operating the OARO process at 50 bar instead of 60 bar while operating at the same long-term water flux.

3.3. Effect of the membrane properties on OARO fouling

Membrane-independent limiting flux in OARO. In this subsection, two different membranes were tested to determine the effect of membrane properties on OARO fouling and flux behaviour (operated in AL-FS mode). In Figure 4, the water flux trends of the AQP and BW30LE membrane are presented for test case F5 (Table 1). The AQP and BW30LE membranes were operated at respective pressures of 50 bar and 40 bar to ensure that the initial water fluxes are comparable and exceed 20 LMH. At this high initial water flux, the BW30LE membrane experienced extremely severe ICP due to the large S value of its substrate. Thus,

the draw solution could not significantly enhance the driving force and therefore, the BW30LE membrane was operated almost in RO process (Refer to Figure S1 in the SI). As shown in the figure, the water fluxes of both membranes converged to the same pseudo-stable water flux of approximately 9 LMH, which was previously determined to be the limiting flux. Hence, the presented results in Figure 4 align with the hypothesis that the OARO limiting flux may be independent of the membrane properties when operated in AL-FS mode. This hypothesis of an OARO membrane-independent limiting flux would be consistent with the observations from conventional RO/NF [17,56] processes and FO processes operated in AL-FS orientation [21].

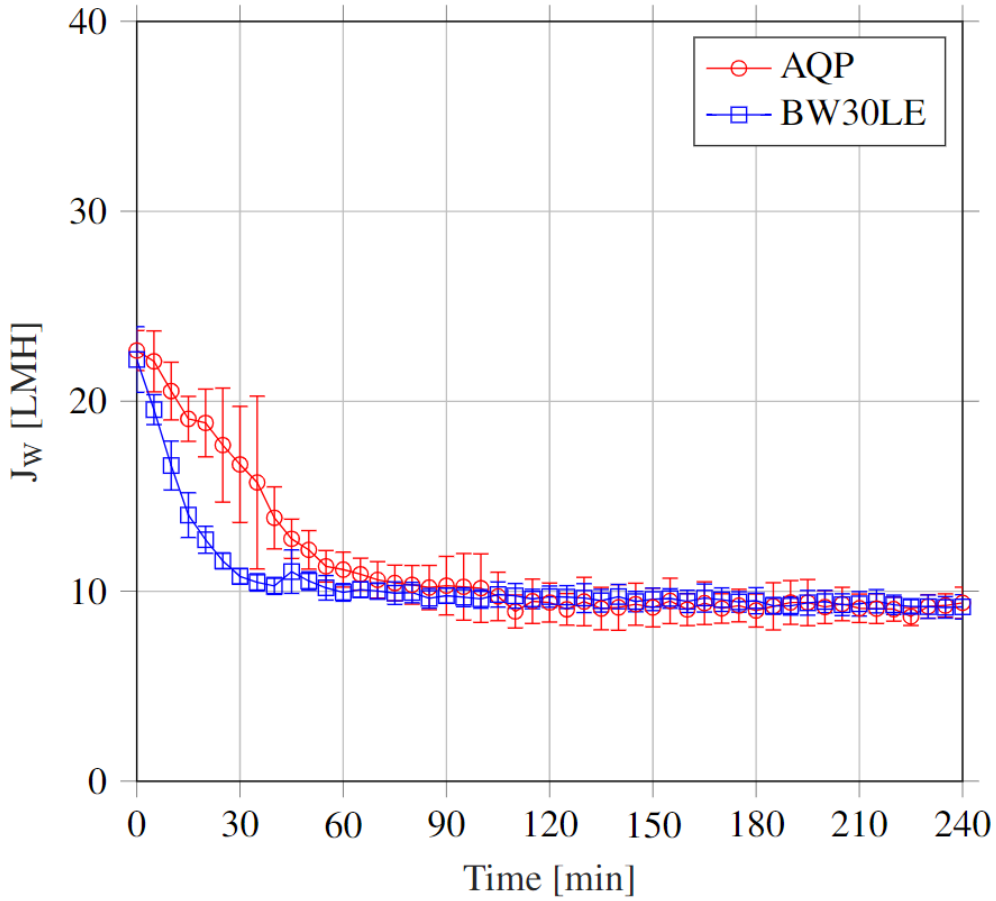

Figure 4: Effect of the membrane properties on OARO permeate flux evolution. All fouling experiments were carried out using the solutions specified for test case F5 in Table 1. The AQP and BW30LE membrane were operated at 50 bar and 40 bar, respectively.

Membrane-dependent ICP self-compensation effect. Although both membranes achieved the same limiting flux, the flux reduction rate differed between the two. While the flux stabilised

for the BW30LE membrane after 1 hour of alginate addition to the feed and draw solutions, the flux of the AQP membrane only stabilised after approximately 1.5 hours. Hence, it seems that the BW30LE membrane is more prone to fouling but in fact, the slower flux reduction of the AQP membrane can be attributed to a stronger ICP-self compensation effect – any minute reduction in the membrane's water flux due to fouling will immediately be counterbalanced by a reduction in ICP [27].

The dilutive concentration polarisation factor f_{DCP} is modelled in Figure 5 (a) and the effective driving force DF_{Eff} is plotted in Figure 5 (b) for the given test case. All terms included in Equation (1) and Equation **Error! Reference source not found.** were calculated using the time varying results with π_F and π_D also changing due to respective concentration of feed solution and dilution of draw solution as the experiment progressed. If f_{DCP} equals 1, the contribution of the draw solution towards the overall driving force is basically nullified and the process is conventional RO. On the other hand, if f_{DCP} equals 0 then the draw solution fully contributes towards the overall driving force, which is ideal for osmotically driven membrane processes. The membrane properties (water permeability A, solute permeability B and structural parameter S) stated in Peters et al. [8] for the AQP membrane at 50 bar ($A = 2.13\ LMH\ bar^{-1}$, $B = 1.56\ LMH$, $S = 809\mu m$) and for the BW30LE membrane at 40 bar ($A = 6.41\ LMH\ bar^{-1}$, $B = 2.24\ LMH$, $S = 2100\mu m$) were used to calculate the change in f_{DCP} for both membranes under the given fouling conditions. As shown in Figure 5 (a), f_{DCP} of the AQP membrane reduces more significantly than that of the BW30LE membrane with the progress of the fouling test. Furthermore, Figure 5 (b) shows that the effective driving force of the AQP membrane increases by approximately 15 bar, whereas that of the BW30LE membrane only increases by roughly 9 bar. This showcases the stronger ICP self-compensation effect of the AQP membrane at higher operational water fluxes ($J_W > 4\ LMH$) due to its smaller structural parameter. It should be noted that the AQP membrane may also experience

a weaker ICP self-compensation effect in the relatively low flux regime ($J_W \leq 4\ LMH$), but this is not the case in our study (refer to S4 in SI).

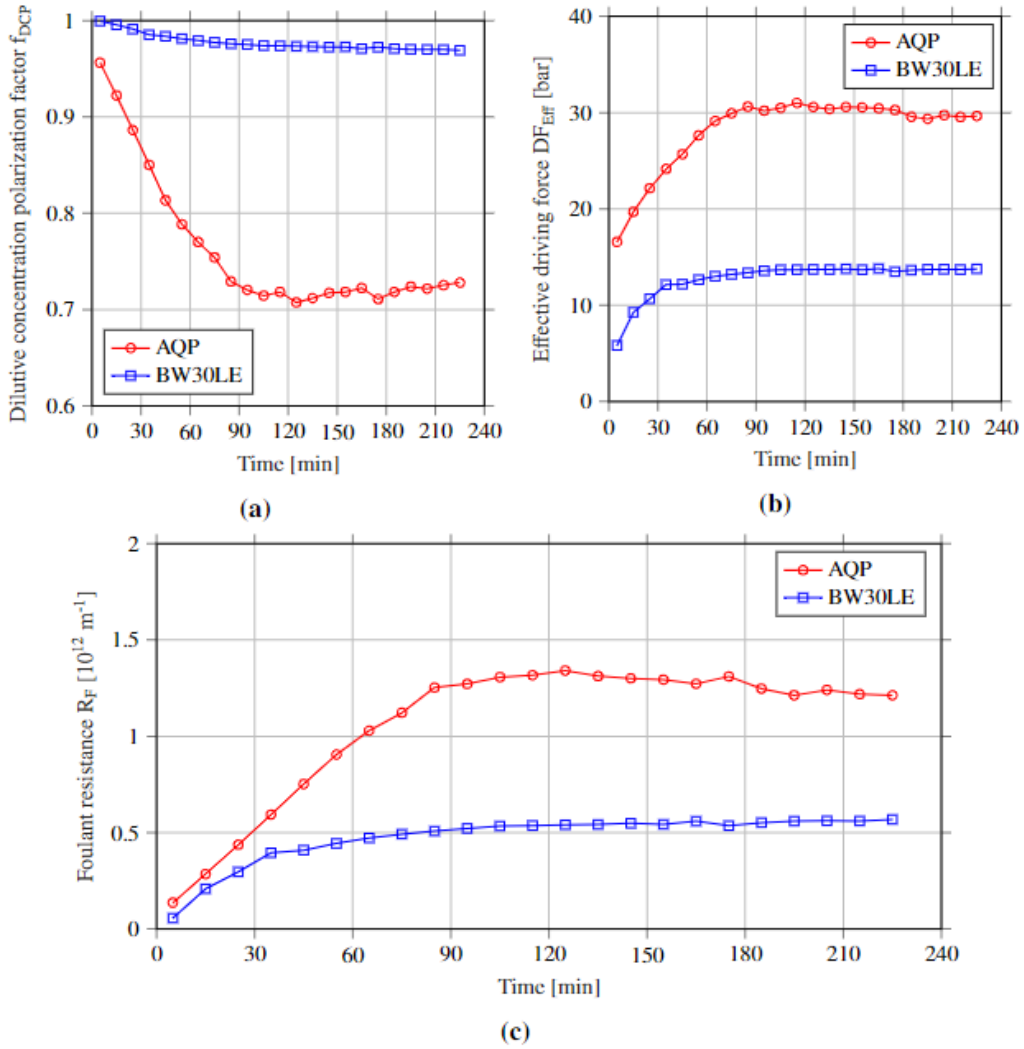

Figure 5: (a) Visualisation of the ICP self-compensation effect for the AQP and BW30LE membrane using the change of f_{DCP} as indicator, (b) the change of the effective driving force with fouling progression, and (c) the calculated foulant resistance of both membranes during the F5 fouling scenario.

This difference in the f_{DCP} trends shows that the membrane properties play a vital role during the transient flux decline period (Approximately the first 1.5 hours of operation). Differences in the AQP membrane morphology (surface roughness: 96 nm [57], surface charge: -45 mV (pH=7) [57], -41 mV (pH=5.3)[58], contact angle: 53° [57], 58.6° [58], 68.2° [59]) and that of the BW30LE membrane (surface roughness: 53 nm, surface charge: -30 mV (pH=6.5), contact angle: 42°)[60] are another cause for the different fouling propensities especially at the early stage of fouling

where foulant-membrane interaction plays an important role, as they directly affect the foulant deposition rate due to differences in membrane-foulant interactions.

Using the membrane properties given in Peters et al. [8] and the given operating conditions in this study, Equation (1) and Equation (3) can be used to calculate the change in the foulant resistance during the experiment. As shown in Figure 5 (c), the foulant resistance of the AQP membrane increased more drastically during the initial stage of the flux decline period than for the BW30LE membrane. The higher fouling resistance of the AQP membrane can be attributed to its higher DF_{Eff} during the experiment [26]. Once the limiting flux is reached for either membrane, R_F remains constant, which shows that a pseudo-stable state is reached in which its foulant resistance remains relatively constant, suggesting additional foulant accumulation on the membrane would not occur.

As observed above, the membrane properties are not important when operating at the limiting flux, but they are still important during the initial stages of the fouling period or when the final pseudo-stable flux is lower than the limiting flux [15,21]. Therefore, the OARO membrane properties are an important consideration when (1) continuous membrane cleaning is considered, or when (2) operating at pressures and feed conditions where the final pseudo-stable flux is below the limiting flux. Depending on the membrane properties, the operating conditions and the feed composition, the critical flux and hence the onset of membrane fouling will differ between the AQP and BW30LE membrane. Thus, the conceptual flux behaviour will differ between the two membranes. Under the given feed and operating conditions, the AQP membrane has a higher fouling propensity than the BW30LE membrane, as shown in Figure 5 (b).

3.4. OARO membrane fouling reversibility

Three cleaning scenarios (i.e., surface flushing, osmotic backwashing using DI water (ideal OB), and osmotic backwashing using non-pure solution (real OB)) were tested on the AQP membrane to investigate the fouling reversibility. The results presented in Figure 6 show that the ideal OB is the best cleaning strategy, which is capable of fully restoring the initial water flux in OARO. Similarly, the ideal OB approach also exhibited high cleaning efficiency for the BW30LE membrane (Refer to S6 in SI), despite its lower back washing flux and different membrane properties from that of the AQP membrane. This high flux recovery can be related to the relatively weak interaction between alginate and the membrane surface, as alginate is of a hydrophilic nature. In addition, larger aggregates were formed when calcium ions bound the carboxylic functional groups of adjacent alginate macromolecules. Hence, the larger alginate aggregates were easily loosened from the membrane surface due to the lifting force created by the backwash permeation. The loosened cake/gel layer was then fully removed from the membrane surface by the shear-induced erosion caused by the cross-flow velocity on the membrane's feed side [61]. This finding is consistent with those made in prior studies on the reversibility of alginate fouling in FO [61,62]. In another study, Blandin et al. [41] found that although osmotic backwashing effectively removed alginate and humic acid aggregates from the membrane surface, the dislodged foulants would not be effectively removed from the feed channel at low CFV (10 cm/s). Instead Blandin et al. [41] found they had to use a higher CFV of 0.35 m/s to fully remove the foulants from the feed channel. This issue was not observed during our OB experiments, which were carried out at a CFV of 10 cm/s, as no feed spacer was employed.

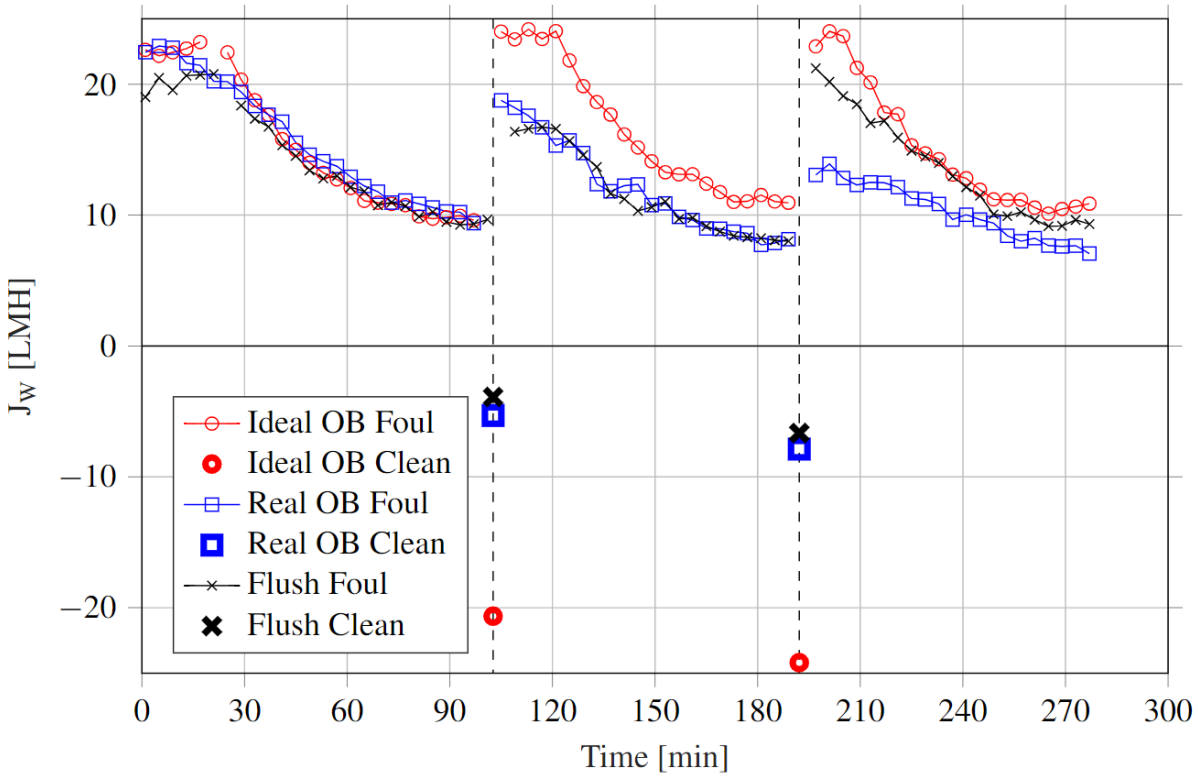

Figure 6: The effectiveness of the three cleaning scenarios. Ideal OB: Osmotic backwash using 2.4M NaCl feed and DI water as draw. Real OB: Osmotic backwash using OARO brine as feed and draw according to test case F5 (Table 1). Flush: surface flushing using DI water as feed and draw solution. The different cleaning conditions are specified in Section 0 and Section S1 in the SI. All fouling experiments were carried out using the solutions specified for test case F5 in Table 1. The AQP membrane was operated at 50 bar with a CFV of 10 cm/s during the fouling cycles. Each of the three fouling cycles lasted 80 min, to give a total fouling duration of 4 hours whereas each cleaning cycle lasted 10 minutes. The negative flux in the figure indicates that the direction of flux is reversed during cleaning.

In comparison to the ideal OB, the initial water flux could not be fully restored using the real OB. The initial water flux decreased for each subsequent fouling cycle, indicating that the foulant resistance R_F increased cumulatively after each fouling and cleaning cycle. As would be expected, using saline draw solutions lowered the reverse water flux, as shown in Figure 6. This in turn meant that the hydrodynamic drag force used to detach the foulants from the membrane surface was lowered. Moreover, as the permeating flux was momentarily reversed during OB, foulants from the draw solution could have be drawn into the membrane substrate, which can cause pore blockage. In this case, removing the deposited foulants within the membrane substrate could be difficult even after the direction of the OARO operational water

flux is restored after cleaning. Pore blockage was observed by several researchers and is generally regarded as irreversible [61–64]. Therefore, cleaning of the OARO membrane is not advised using impure draw solutions. On-line osmotic backwashing of the OARO membrane is therefore not recommended if impure draw solutions are to be utilised.

While the efficiency between the different flushing cycles seems to differ, membrane flushing is still deemed more effective than real OB. As previously mentioned, the calcium alginate aggregates cause a severe flux decline during OARO operation, but these are easily removed from the membrane surface due to their large size. It is also important to mention that although the membrane was flushed with deionised feed and draw solutions, a reverse water flux was still generated (as shown in Figure 6), which may have improved the flushing efficiency. Similarly, Kim et al. also observed a reverse water flux during surface flushing [62]. This backwashing water flux can be attributed to the cake enhanced concentration polarisation (CECP) phenomenon. Generally, ions are trapped between the membrane's active layer and the adjacent foulant layer due to CECP. Once the draw and feed solutions are swapped from the fouling solutions to the deionised solutions, these ions are still trapped in the foulant layer and cause a transmembrane osmotic pressure difference from feed to draw side. Hence, reverse water permeation is induced during membrane flushing. This is beneficial in the sense that simple membrane flushing induces a reverse water flux that helps to dislodge the cake/gel layer from the membrane surface. However, the magnitude of the backwash water flux is not constant between cleaning cycles and its duration is relatively short. This may explain the varying efficiency of membrane flushing.

4. Implications

This study is the first published to our knowledge to systematically investigate fouling in the OARO membrane process. The presented findings offer insights into (1) the fouling mechanisms occurring during OARO operation, and (2) the impacts of membrane fouling on

561 the process performance. Furthermore, the presented results offer guidance for OARO
562 operation under extreme operating conditions with harsh feed and draw solutions. The
563 following conclusions highlight the findings of the study:

564 • The presented results suggest that the limiting flux may be independent of the OARO
565 membrane properties. However, the membrane properties play a vital role (1) when
566 operating at pseudo-stable fluxes below the limiting flux, (2) during the initial stages
567 of fouling when the limiting flux has not yet been reached, and (3) during membrane
568 cleaning.
569 o The AQP membrane with a thinner substrate experiences a higher fouling
570 resistance due to its stronger ICP self-compensation effect in the high operating
571 flux region.
572 o Membranes with a thinner substrate are preferred for osmotic backwashing or
573 flushing, as a higher backwash flux can be achieved during membrane cleaning.
574 • Long-term OARO operation at 50 bar is more energy efficient than at 60 bar for the
575 given feed composition, as the same pseudo-stable flux (limiting flux) is achieved at
576 both pressures.
577 • For an AL-FS orientation, fouling on the membrane's draw side was found to be
578 negligible during OARO operation. Fouling mainly occurred due to the formation of a
579 cake/gel layer on the membrane's active layer on the feed side.
580 o Hence, impure draw solutions could be potentially used for OARO operation at
581 low risk of membrane fouling. However, fouling and plugging of the draw
582 channel can increase the draw side pressure loss.
583 o Conversely, using impure draw solutions prohibits the use of on-line osmotic
584 backwashing, as foulants may enter the membrane's substrate during cleaning
585 and cause irreversible membrane fouling. In addition, using saline draw

586 solutions during backwashing lowers the reverse water flux and hence, lowers
587 the OB cleaning efficacy.
588 • Fouling by alginate in the presence of calcium ions is severe during OARO operation.
589 This fouling layer is, however, easily detachable from the membrane. To prevent severe
590 membrane fouling in OARO, continuous membrane cleaning is required, or the feed
591 solution must be softened and/or alginate removed.
592

Associated Content

Supporting Information

(S1) AQP and BW30LE reference case simulations, (S2) Plugged OARO draw spacer, (S3) The limiting flux, (S4) The ICP self-compensation effect at different water fluxes, (S5) Foulant resistance at different operating pressures, and (S6) Ideal OB of the AQP and BW30LE membrane.

Acknowledgements

This research was supported by the Start-up Grant (SUG #002195-00001) for Q.S. from Nanyang Technological University. C.D. Peters would like to thank the Singapore Membrane Technology Centre (SMTC) at Nanyang Technological University for hosting a four-month research stay to carry out this research. Furthermore, C.D. Peters and N.P. Hankins are grateful to the University of Bahrain (in the Kingdom of Bahrain) for granting a full scholarship to C.D. Peters.

References

(1) Bartholomew, T. V; Mey, L.; Arena, J. T.; Siefert, N. S.; Mauter, M. S. Osmotically Assisted Reverse Osmosis for High Salinity Brine Treatment. *Desalination* **2017**, *421*, 3–11. https://doi.org/https://doi.org/10.1016/j.desal.2017.04.012.

(2) Chen, X.; Yip, N. Y. Unlocking High-Salinity Desalination with Cascading Osmotically Mediated Reverse Osmosis: Energy and Operating Pressure Analysis. *Environ. Sci. Technol.* **2018**, *52* (4), 2242–2250. https://doi.org/10.1021/acs.est.7b05774.

(3) Bartholomew, T. V.; Siefert, N. S.; Mauter, M. S. Cost Optimization of Osmotically Assisted Reverse Osmosis. *Environ. Sci. Technol.* **2018**. https://doi.org/10.1021/acs.est.8b02771.

(4) Peters, C. D.; Hankins, N. P. Osmotically Assisted Reverse Osmosis (OARO): Five Approaches to Dewatering Saline Brines Using Pressure-Driven Membrane Processes. *Desalination* **2019**. https://doi.org/10.1016/j.desal.2019.01.025.

(5) Bouma, A. T.; Lienhard, J. H. Split-Feed Counterflow Reverse Osmosis for Brine Concentration. *Desalination* **2018**, *445*, 280–291. https://doi.org/10.1016/J.DESAL.2018.07.011.

(6) Peters, C. D.; Hankins, N. P. The Synergy between Osmotically Assisted Reverse Osmosis (OARO) and the Use of Thermo-Responsive Draw Solutions for Energy Efficient, Zero-Liquid Discharge Desalination. *Desalination* **2020**, *493*, 114630. https://doi.org/10.1016/j.desal.2020.114630.

(7) Mo, Z.; Peters, C. D.; Long, C.; Hankins, N. P.; She, Q. How Split-Feed Osmotically Assisted Reverse Osmosis (SF-OARO) Can Outperform Conventional Reverse Osmosis (CRO) Processes under Constant and Varying Electricity Tariffs. *Desalination* **2022**, *530*, 115670. https://doi.org/10.1016/J.DESAL.2022.115670.

(8) Peters, C. D.; Ng, D. Y. F.; Hankins, N. P.; She, Q. A Novel Method for the Accurate Characterization of Transport and Structural Parameters of Deformable Membranes Utilized in Pressure- and Osmotically Driven Membrane Processes. *J. Memb. Sci.* **2021**, *638*, 119720. https://doi.org/10.1016/J.MEMSCI.2021.119720.

(9) Kim, J.; Kim, D. I.; Hong, S. Analysis of an Osmotically-Enhanced Dewatering Process for the Treatment of Highly Saline (Waste)Waters. *J. Memb. Sci.* **2018**, *548*, 685–693. https://doi.org/https://doi.org/10.1016/j.memsci.2017.10.048.

(10) She, Q.; Wang, R.; Fane, A. G.; Tang, C. Y. Membrane Fouling in Osmotically Driven Membrane Processes: A Review. *J. Memb. Sci.* **2016**, *499*, 201–233. https://doi.org/10.1016/j.memsci.2015.10.040.

(11) Zohrabian, L.; Hankins, N. P.; Field, R. W. Hybrid Forward Osmosis-Membrane Distillation System: Demonstration of Technical Feasibility. *J. Water Process Eng.* **2020**, *33*, 101042. https://doi.org/10.1016/j.jwpe.2019.101042.

(12) Boo, C.; Elimelech, M.; Hong, S. Fouling Control in a Forward Osmosis Process Integrating Seawater Desalination and Wastewater Reclamation. *J. Memb. Sci.* **2013**, *444*, 148–156. https://doi.org/10.1016/j.memsci.2013.05.004.

(13) Kim, Y. C.; Elimelech, M. Adverse Impact of Feed Channel Spacers on the Performance of Pressure Retarded Osmosis. *Environ. Sci. Technol.* **2012**, *46* (8),

650 4673–4681. https://doi.org/10.1021/es3002597.

651 (14) She, Q.; Wong, Y. K. W.; Zhao, S.; Tang, C. Y. Organic Fouling in Pressure Retarded
652 Osmosis: Experiments, Mechanisms and Implications. *J. Memb. Sci.* **2013**, *428*, 181–
653 189. https://doi.org/10.1016/j.memsci.2012.10.045.

654 (15) Bacchin, P.; Aimar, P.; Field, R. W. Critical and Sustainable Fluxes: Theory,
655 Experiments and Applications. *J. Memb. Sci.* **2006**, *281* (1), 42–69.
656 https://doi.org/https://doi.org/10.1016/j.memsci.2006.04.014.

657 (16) Bacchin, P. A Possible Link between Critical and Limiting Flux for Colloidal Systems:
658 Consideration of Critical Deposit Formation along a Membrane. In *Journal of*
659 *Membrane Science*; Elsevier, 2004; Vol. 228, pp 237–241.
660 https://doi.org/10.1016/j.memsci.2003.10.012.

661 (17) Tang, C. Y.; Leckie, J. O. Membrane Independent Limiting Flux for RO and NF
662 Membranes Fouled by Humic Acid. *Environ. Sci. Technol.* **2007**, *41* (13), 4767–4773.
663 https://doi.org/10.1021/es063105w.

664 (18) Gu, Y.; Wang, Y.-N.; Wei, J.; Tang, C. Y. Organic Fouling of Thin-Film Composite
665 Polyamide and Cellulose Triacetate Forward Osmosis Membranes by Oppositely
666 Charged Macromolecules. *Water Res.* **2013**, *47* (5), 1867–1874.
667 https://doi.org/https://doi.org/10.1016/j.watres.2013.01.008.

668 (19) Zhang, M.; Hou, D.; She, Q.; Tang, C. Y. Gypsum Scaling in Pressure Retarded
669 Osmosis: Experiments, Mechanisms and Implications. *Water Res.* **2014**, *48*, 387–395.
670 https://doi.org/10.1016/j.watres.2013.09.051.

671 (20) Tang, C. Y.; Chong, T. H.; Fane, A. G. Colloidal Interactions and Fouling of NF and
672 RO Membranes: A Review. *Advances in Colloid and Interface Science*. Elsevier B.V.
673 May 11, 2011, pp 126–143. https://doi.org/10.1016/j.cis.2010.10.007.

674 (21) Morrow, C. P.; Childress, A. E. Evidence, Determination, and Implications of
675 Membrane-Independent Limiting Flux in Forward Osmosis Systems. *Environ. Sci.*
676 *Technol.* **2019**, *53* (8), 4380–4388. https://doi.org/10.1021/acs.est.8b05925.

677 (22) She, Q.; Zhang, L.; Wang, R.; Krantz, W. B.; Fane, A. G. Pressure-Retarded Osmosis
678 with Wastewater Concentrate Feed: Fouling Process Considerations. *J. Memb. Sci.*
679 **2017**, *542*, 233–244. https://doi.org/10.1016/j.memsci.2017.08.022.

680 (23) Fei, J.; Mai, W.; Cheng, P. S.; Shi, J.; Liu, Z.; She, Q. Membrane Structure-Dependent
681 Limiting Flux Behavior and Membrane Selectivity Loss during Gypsum Scaling:
682 Implications for Pressure-Retarded Osmosis Operation and Membrane Design.
683 *Desalination* **2020**, *492*, 114644. https://doi.org/10.1016/j.desal.2020.114644.

684 (24) Zou, S.; Wang, Y. N.; Wicaksana, F.; Aung, T.; Wong, P. C. Y.; Fane, A. G.; Tang, C.
685 Y. Direct Microscopic Observation of Forward Osmosis Membrane Fouling by
686 Microalgae: Critical Flux and the Role of Operational Conditions. *J. Memb. Sci.* **2013**,
687 *436*, 174–185. https://doi.org/10.1016/j.memsci.2013.02.030.

688 (25) Zhang, J.; Loong, W. L. C.; Chou, S.; Tang, C.; Wang, R.; Fane, A. G. Membrane
689 Biofouling and Scaling in Forward Osmosis Membrane Bioreactor. *J. Memb. Sci.*
690 **2012**, *403–404*, 8–14. https://doi.org/10.1016/j.memsci.2012.01.032.

691 (26) Siddiqui, F. A.; She, Q.; Fane, A. G.; Field, R. W. Exploring the Differences between
692 Forward Osmosis and Reverse Osmosis Fouling. *J. Memb. Sci.* **2018**, *565*, 241–253.

https://doi.org/10.1016/j.memsci.2018.08.034.

(27) Tang, C. Y.; She, Q.; Lay, W. C. L.; Wang, R.; Fane, A. G. Coupled Effects of Internal Concentration Polarization and Fouling on Flux Behavior of Forward Osmosis Membranes during Humic Acid Filtration. *J. Memb. Sci.* **2010**, *354* (1–2), 123–133. https://doi.org/10.1016/j.memsci.2010.02.059.

(28) She, Q.; Hou, D.; Liu, J.; Tan, K. H.; Tang, C. Y. Effect of Feed Spacer Induced Membrane Deformation on the Performance of Pressure Retarded Osmosis (PRO): Implications for PRO Process Operation. *J. Memb. Sci.* **2013**, *445*, 170–182. https://doi.org/10.1016/j.memsci.2013.05.061.

(29) Song, Y.; Gao, X.; Gao, C. Evaluation of Scaling Potential in a Pilot-Scale NF–SWRO Integrated Seawater Desalination System. *J. Memb. Sci.* **2013**, *443*, 201–209. https://doi.org/https://doi.org/10.1016/j.memsci.2013.04.048.

(30) Wang, S. Y.; Chen, Y. F.; Zhou, H.; Xu, X. H.; Cheng, L. H. Calcium Carbonate Scaling in Forward Osmosis for Textile Reverse Osmosis Concentrate Treatment. *J. Water Process Eng.* **2020**, *35*, 101181. https://doi.org/10.1016/j.jwpe.2020.101181.

(31) Li, Z.; Valladares Linares, R.; Bucs, S.; Aubry, C.; Ghaffour, N.; Vrouwenvelder, J. S.; Amy, G. Calcium Carbonate Scaling in Seawater Desalination by Ammonia-Carbon Dioxide Forward Osmosis: Mechanism and Implications. *J. Memb. Sci.* **2015**, *481*, 36–43. https://doi.org/10.1016/j.memsci.2014.12.055.

(32) Lee, S.; Kim, Y. C. Calcium Carbonate Scaling by Reverse Draw Solute Diffusion in a Forward Osmosis Membrane for Shale Gas Wastewater Treatment. *J. Memb. Sci.* **2017**, *522*, 257–266. https://doi.org/10.1016/j.memsci.2016.09.026.

(33) Xie, M.; Gray, S. R. Gypsum Scaling in Forward Osmosis: Role of Membrane Surface Chemistry. *J. Memb. Sci.* **2016**, *513*, 250–259. https://doi.org/10.1016/j.memsci.2016.04.022.

(34) Baoxia, M. I.; Elimelech, M. Gypsum Scaling and Cleaning in Forward Osmosis: Measurements and Mechanisms. *Environ. Sci. Technol.* **2010**, *44* (6), 2022–2028. https://doi.org/10.1021/es903623r.

(35) Rahardianto, A.; Mccool, B. C.; Cohen, Y. Reverse Osmosis Desalting of Inland Brackish Water of High Gypsum Scaling Propensity: Kinetics and Mitigation of Membrane Mineral Scaling. *Environ. Sci. Technol.* **2008**, *42* (12), 4292–4297. https://doi.org/10.1021/es702463a.

(36) ASTM D1141 - 98(2008) Standard Practice for the Preparation of Substitute Ocean Water.

(37) Yu, W.; Song, D.; Li, A.; Yang, H. Control of Gypsum-Dominated Scaling in Reverse Osmosis System Using Carboxymethyl Cellulose. *J. Memb. Sci.* **2019**, *577*, 20–30. https://doi.org/10.1016/j.memsci.2019.01.053.

(38) Chauhan, K.; Kumar, R.; Kumar, M.; Sharma, P.; Chauhan, G. S. Modified Pectin-Based Polymers as Green Antiscalants for Calcium Sulfate Scale Inhibition. *Desalination* **2012**, *305*, 31–37. https://doi.org/10.1016/j.desal.2012.07.042.

(39) Mi, B.; Elimelech, M. Organic Fouling of Forward Osmosis Membranes: Fouling Reversibility and Cleaning without Chemical Reagents. *J. Memb. Sci.* **2010**, *348* (1–2), 337–345. https://doi.org/10.1016/j.memsci.2009.11.021.

(40) Vu, M. T.; Ansari, A. J.; Hai, F. I.; Nghiem, L. D. Performance of a Seawater-Driven Forward Osmosis Process for Pre-Concentrating Digested Sludge Centrate: Organic Enrichment and Membrane Fouling. *Environ. Sci. Water Res. Technol.* **2018**, *4* (7), 1047–1056. https://doi.org/10.1039/c8ew00132d.

(41) Blandin, G.; Verliefde, A. R. D.; Le-Clech, P. Pressure Enhanced Fouling and Adapted Anti-Fouling Strategy in Pressure Assisted Osmosis (PAO). *J. Memb. Sci.* **2015**, *493*, 557–567. https://doi.org/10.1016/j.memsci.2015.07.014.

(42) Liberman, B. Three Methods of Forward Osmosis Cleaning for RO Membranes. *Desalination* **2018**, *431*, 22–26. https://doi.org/10.1016/J.DESAL.2017.11.023.

(43) Qin, J. J.; Oo, M. H.; Kekre, K. A.; Liberman, B. Development of Novel Backwash Cleaning Technique for Reverse Osmosis in Reclamation of Secondary Effluent. *J. Memb. Sci.* **2010**, *346* (1), 8–14. https://doi.org/10.1016/j.memsci.2009.08.011.

(44) Li, W.; Su, X.; Palazzolo, A.; Ahmed, S. Numerical Modeling of Concentration Polarization and Inorganic Fouling Growth in the Pressure-Driven Membrane Filtration Process. *J. Memb. Sci.* **2019**, *569*, 71–82. https://doi.org/https://doi.org/10.1016/j.memsci.2018.10.007.

(45) Vrouwenvelder, J. S.; Picioreanu, C.; Kruithof, J. C.; van Loosdrecht, M. C. M. Biofouling in Spiral Wound Membrane Systems: Three-Dimensional CFD Model Based Evaluation of Experimental Data. *J. Memb. Sci.* **2010**, *346* (1), 71–85. https://doi.org/10.1016/J.MEMSCI.2009.09.025.

(46) Antony, A.; Low, J. H.; Gray, S.; Childress, A. E.; Le-Clech, P.; Leslie, G. Scale Formation and Control in High Pressure Membrane Water Treatment Systems: A Review. *J. Memb. Sci.* **2011**, *383* (1), 1–16. https://doi.org/https://doi.org/10.1016/j.memsci.2011.08.054.

(47) Chen, S. C.; Wan, C. F.; Chung, T. S. Enhanced Fouling by Inorganic and Organic Foulants on Pressure Retarded Osmosis (PRO) Hollow Fiber Membranes under High Pressures. *J. Memb. Sci.* **2015**, *479*, 190–203. https://doi.org/10.1016/j.memsci.2015.01.037.

(48) Liu, Y.; Mi, B. Combined Fouling of Forward Osmosis Membranes: Synergistic Foulant Interaction and Direct Observation of Fouling Layer Formation. *J. Memb. Sci.* **2012**, *407–408*, 136–144. https://doi.org/10.1016/j.memsci.2012.03.028.

(49) Mi, B.; Elimelech, M. Chemical and Physical Aspects of Organic Fouling of Forward Osmosis Membranes. *J. Memb. Sci.* **2008**, *320* (1–2), 292–302. https://doi.org/10.1016/j.memsci.2008.04.036.

(50) Tang, C. Y.; Kwon, Y. N.; Leckie, J. O. Fouling of Reverse Osmosis and Nanofiltration Membranes by Humic Acid-Effects of Solution Composition and Hydrodynamic Conditions. *J. Memb. Sci.* **2007**, *290* (1–2), 86–94. https://doi.org/10.1016/j.memsci.2006.12.017.

(51) Guha, R.; Shang, X.; Zydney, A. L.; Velegol, D.; Kumar, M. Diffusiophoresis Contributes Significantly to Colloidal Fouling in Low Salinity Reverse Osmosis Systems. *J. Memb. Sci.* **2015**, *479*, 67–76. https://doi.org/10.1016/J.MEMSCI.2015.01.024.

(52) She, Q.; Tang, C. Y.; Wang, Y. N.; Zhang, Z. The Role of Hydrodynamic Conditions

and Solution Chemistry on Protein Fouling during Ultrafiltration. *Desalination* **2009**, *249* (3), 1079–1087. https://doi.org/10.1016/j.desal.2009.05.015.

(53) Xia, L.; Andersen, M. F.; Hélix-Nielsen, C.; McCutcheon, J. R. Novel Commercial Aquaporin Flat-Sheet Membrane for Forward Osmosis. *Ind. Eng. Chem. Res.* **2017**, *56* (41), 11919–11925. https://doi.org/10.1021/acs.iecr.7b02368.

(54) Chun, Y.; Qing, L.; Sun, G.; Bilad, M. R.; Fane, A. G.; Chong, T. H. Prototype Aquaporin-Based Forward Osmosis Membrane: Filtration Properties and Fouling Resistance. *Desalination* **2018**, *445*, 75–84. https://doi.org/10.1016/j.desal.2018.07.030.

(55) Singh, N.; Petrinic, I.; Hélix-Nielsen, C.; Basu, S.; Balakrishnan, M. Concentrating Molasses Distillery Wastewater Using Biomimetic Forward Osmosis (FO) Membranes. *Water Res.* **2018**, *130*, 271–280. https://doi.org/10.1016/J.WATRES.2017.12.006.

(56) Tang, C. Y.; Kwon, Y. N.; Leckie, J. O. The Role of Foulant-Foulant Electrostatic Interaction on Limiting Flux for RO and NF Membranes during Humic Acid Fouling-Theoretical Basis, Experimental Evidence, and AFM Interaction Force Measurement. *J. Memb. Sci.* **2009**, *326* (2), 526–532. https://doi.org/10.1016/j.memsci.2008.10.043.

(57) Balkenov, A.; Anuarbek, A.; Satayeva, A.; Kim, J.; Inglezakis, V.; Arkhangelsky, E. Complex Organic Fouling and Effect of Silver Nanoparticles on Aquaporin Forward Osmosis Membranes. *J. Water Process Eng.* **2020**, *34*, 101177. https://doi.org/10.1016/j.jwpe.2020.101177.

(58) Nikbakht Fini, M.; Madsen, H. T.; Sørensen, J. L.; Muff, J. Moving from Lab to Pilot Scale in Forward Osmosis for Pesticides Rejection Using Aquaporin Membranes. *Sep. Purif. Technol.* **2020**, *240*, 116616. https://doi.org/10.1016/j.seppur.2020.116616.

(59) Xie, M.; Luo, W.; Guo, H.; Nghiem, L. D.; Tang, C. Y.; Gray, S. R. Trace Organic Contaminant Rejection by Aquaporin Forward Osmosis Membrane: Transport Mechanisms and Membrane Stability. *Water Res.* **2018**, *132*, 90–98. https://doi.org/10.1016/j.watres.2017.12.072.

(60) Widjaya, A.; Hoang, T.; Stevens, G. W.; Kentish, S. E. A Comparison of Commercial Reverse Osmosis Membrane Characteristics and Performance under Alginate Fouling Conditions. *Sep. Purif. Technol.* **2012**, *89*, 270–281. https://doi.org/10.1016/j.seppur.2012.01.038.

(61) Motsa, M. M.; Mamba, B. B.; Thwala, J. M.; Verliefde, A. R. D. Osmotic Backwash of Fouled FO Membranes: Cleaning Mechanisms and Membrane Surface Properties after Cleaning. *Desalination* **2017**, *402*, 62–71. https://doi.org/10.1016/j.desal.2016.09.018.

(62) Kim, C.; Lee, S.; Hong, S. Application of Osmotic Backwashing in Forward Osmosis: Mechanisms and Factors Involved. *Desalin. Water Treat.* **2012**, *43* (1–3), 314–322. https://doi.org/10.1080/19443994.2012.672215.

(63) Yip, N. Y.; Elimelech, M. Influence of Natural Organic Matter Fouling and Osmotic Backwash on Pressure Retarded Osmosis Energy Production from Natural Salinity Gradients. *Environ. Sci. Technol.* **2013**, *47* (21), 12607–12616. https://doi.org/10.1021/es403207m.

(64) Kim, J. E.; Phuntsho, S.; Lotfi, F.; Shon, H. K. Investigation of Pilot-Scale 8040 FO Membrane Module under Different Operating Conditions for Brackish Water Desalination. *Desalin. Water Treat.* **2015**, *53* (10), 2782–2791. https://doi.org/10.1080/19443994.2014.931528.

829 **For Table of Contents Only**

830

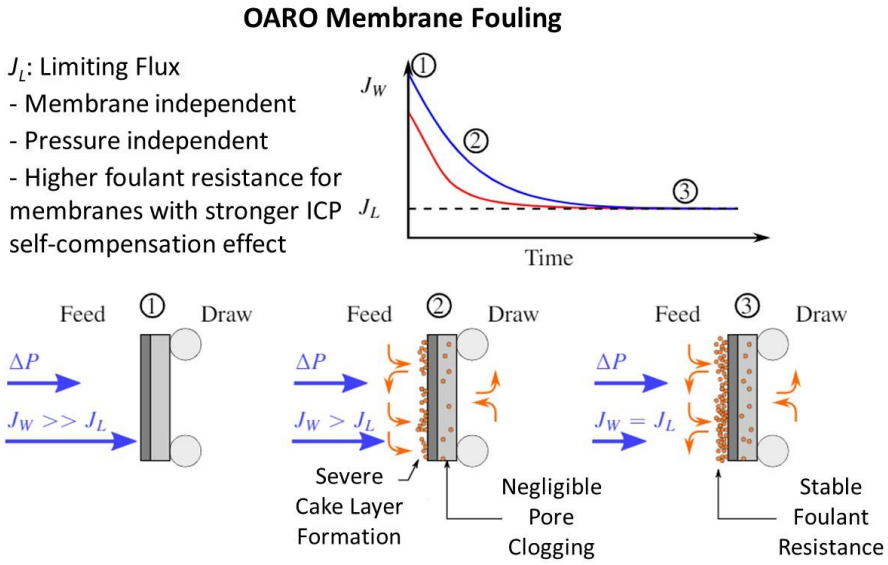

831

832